

A new analysis of quasar polarisation alignments

V. Pelgrims^{1*} and J.R. Cudell^{1†}

¹IFPA, AGO dept., University of Liège, B4000 Liège, Belgium

6th May 2019

Abstract

We propose a new method to analyse the alignment of optical polarisation vectors from quasars. This method allows a precise determination of the deviation from a random distribution, and defines intrinsic preferred axes. The global significance of the effect is found to be as low as $3 \cdot 10^{-5}$.

1 Introduction

Fifteen years ago, Hutsemékers discovered that the optical polarisation vectors from distant quasars are not randomly distributed [Hutsemékers 1998]. The original study considered a sample of 170 quasars, and the probability of a random distribution was 0.5 %. Since then, further measurements have been added [Hutsemékers & Lamy, 2001, Sluse et al. 2005, Hutsemékers et al. 2005], and the significance of the effect has grown: with the present sample of 355 polarisation data points, the alignment effect has been estimated to have a probability lower than 0.1 % in some regions of the sky defined by cuts on right ascension and redshift.

The original test had however a weak point, as the angles of the polarisation vectors are measured with respect to their local meridian. Therefore, the strength of the alignment, and the significance of the effect, depend on the choice of the spherical coordinate system, so that it is possible to find an axis for which the effect becomes negligible, i.e. for which the data look random. Indeed, the original statistical tests do not take into account the fact that polarisation vectors come from different lines of sight and thus are not defined in the same plane. To remedy this problem, [Jain, Narain & Sarala, 2004] have proposed to parallel-transport the polarisation vectors along geodesics of the celestial sphere onto one point in order to compare them. While the distribution of polarisation angles still depends on the point where it is built, it does not depend on the coordinates, and one can build robust statistical tests (see Jain et al. (2004) and Hutsemékers et al. (2005)). Unfortunately, these tests have to resort to the generation of a large number of random data in order to determine the significance of the signal and do not lead to a clear characterization of the effect. Furthermore, to make an intrinsic test, polarisation vectors must be transported to the location of the quasars. However, this is an arbitrary choice as they can be transported to any point of the celestial sphere. The sum of the parallel-transported polarisation vectors then makes a continuous axial vector field on the sphere, and by the hairy ball theorem [Eisenberg & Guy, 1979], it is still possible to find at least two points where the effect vanishes. Hence the quantification of the size of the effect seems again uncertain.

We propose here another method which is totally independent of the coordinate system, and which quantifies unambiguously the alignment effect. It allows us to compare the polarisation vectors of sources located at different angular coordinates and leads to the characterization of the effect through a blind analysis of the data. The basic idea is to consider the physical polarisation vectors as 3-dimensional objects rather than 2-dimensional ones embedded in their polarisation plane. These 3-dimensional objects are the directions of the electric field oscillations and they are the physical objects which are measured. As we are dealing with a number of vectors, it is clear that it will be possible to define preferred directions. We can also use the same method to study the dependence on redshift, position in the sky or strength of polarisation by imposing cuts on these variables and repeating the study for a sub-sample.

We devote the present paper to the construction of this new statistical method applied here to the analysis of quasar polarisation data, in which the evaluation of the significance of the signal will be largely analytic. The second section of this paper explains the details of our statistical method. It also contains illustrations and discussions related to the statistical background, when polarisation angles are assumed to be uniformly distributed, and is compared with the original studies of [Hutsemékers 1998, Hutsemékers & Lamy, 2001,

*pelgrims@astro.ulg.ac.be

†jr.cudell@ulg.ac.be

Hutsemékers et al. 2005, Hutsemékers et al. 2008, Hutsemékers et al. 2010] using the same cuts. The third section is devoted to the application of this new statistical method first globally, then to slices in redshift. We also consider there the dependence of the alignment on the various parameters, the possibility of a cosmological alignment, and define our final most significant regions exhibiting an anomalous alignment of polarisation vectors.

2 A coordinate-invariant statistical test for polarisation data

When an electromagnetic wave is partially or fully linearly polarized, a polarisation vector is introduced. Its norm reflects the degree of linear polarisation of the radiation while its direction is that of the oscillating electric field. This vector is thus embedded into the plane orthogonal to the radiation direction of propagation, the polarisation plane. Since the electric field is oscillating, the polarisation vector is an axial quantity, rather than a true vector, so that the polarisation angle is determined up to π radians.

We consider sources as being points on the unit celestial sphere and we choose a spherical polar coordinate system defined by the orthonormal 3-vectors $(\mathbf{e}_r, \mathbf{e}_\theta, \mathbf{e}_\phi)$, with \mathbf{e}_θ pointing to the South pole. In the following bold-faced letters indicate 3-vectors. Polarisation vectors are tangent to this unit sphere. For a given source in the direction \mathbf{e}_r , a polarisation vector must lie in the plane defined by the two unit vectors \mathbf{e}_ϕ and \mathbf{e}_θ . We choose the angle ψ between the polarisation vector \mathbf{p} and the basis vector \mathbf{e}_ϕ , defined in the range $[-\pi/2, \pi/2]$, to be the polarisation angle. The normalized polarisation vector can then be written

$$\hat{\mathbf{p}} = \cos\psi \mathbf{e}_\phi - \sin\psi \mathbf{e}_\theta . \quad (1)$$

Each measurement (i) of the dataset [Hutsemékers et al. 2005] is equivalent to a position 3-vector $\mathbf{e}_r^{(i)}$ associated with a normalised polarisation direction $\hat{\mathbf{p}}^{(i)}$ and polarisation magnitude $|\mathbf{p}^{(i)}|$. Contrarily to the various angles, $\mathbf{e}_r^{(i)}$ and $\hat{\mathbf{p}}^{(i)}$ are physical, *i.e.* they do not depend on the choice of coordinates. As we are interested in polarisation alignments, we shall consider mostly the $\hat{\mathbf{p}}^{(i)}$ in the following.

The problem is then as follows: we have a number of normalised vectors, and we want to decide if they are abnormally aligned. We can draw them from the same origin, and their ends, which we shall call the polarisation points, have to lie on a unit 2-sphere, which we shall refer to as the polarisation sphere. The problem is that the sphere is not uniformly covered by the points. Indeed, for each source, the polarisation vectors are constrained to be in the plane defined by the basis vectors $(\mathbf{e}_\phi^{(i)}, \mathbf{e}_\theta^{(i)})$. The intersection between the plane and the polarisation sphere is a great circle, which is the geometric locus where the polarisation vector attached to the source (i) may intersect the sphere, as shown in Fig. 1. Note that the figure is symmetric as polarisation vectors are defined up to a sign. In the following, we choose to show the full sphere, although a half-sphere could be used to represent the polarisation space.

To compare the observational data with a random distribution of polarisation points, we need to select a region on the polarisation sphere, count the number of polarisation points, and compare with what one would get from a uniform random distribution along the locus of the polarisation points for fixed position vectors. One could do this by Monte-Carlo techniques, but as we shall see the probabilities turn out to be rather low, so that a detailed study would prove difficult.

However, we found that a particular choice of shape for the region on the sphere considerably simplifies the evaluation of probabilities. We consider cones in which the polarisation vectors fall, or equivalently spherical caps of fixed aperture angle. The probability distribution of a given number of points in a given spherical cap can be computed analytically as explained below. A scan of the whole polarisation half-sphere leads to a map of expected densities which constitutes the statistical background. At any location on the half-sphere, the hypothesis of uniformity can then be tested by calculating the probability of the observed number of polarisation points. An alignment of polarisation vectors from different sources will be detected when an over-density between data points and the background is significant.

2.1 Construction of the probability distribution

As mentioned above, the locus of the polarisation points is a half-circle in the plane normal to the source position vector. The probability that a polarisation point lies inside a spherical cap is then given by the length of the arc of circle intercepted by the cap, divided by the whole length of the half-circle (π). Let η being the half-aperture angle of the spherical cap, and $\hat{\mathbf{s}}$ the unit vector pointing to its centre. If $\hat{\mathbf{p}}^{(i)}$ is a normalised polarisation vector attached to the source (i) , with position vector $\mathbf{e}_r^{(i)}$, the corresponding polarisation point lies inside the spherical cap centred at $\hat{\mathbf{s}}$ if and only if

$$|\hat{\mathbf{p}}^{(i)} \cdot \hat{\mathbf{s}}| \geq \cos\eta \quad (2)$$

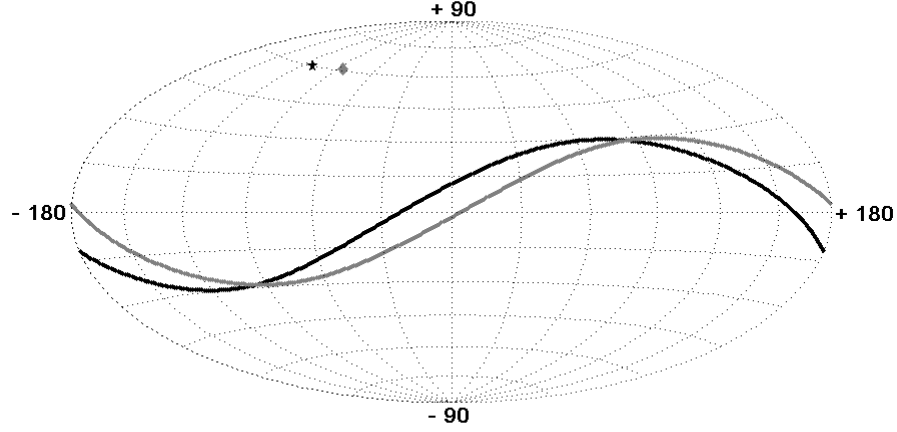


Figure 1: Superposition of the Hammer-Aitoff projections of the celestial sphere and the polarisation sphere (in galactic coordinates). Two quasars (B1115+080 (in black) and B1157+014 (in grey)) are displayed on the celestial sphere with the corresponding geometric loci of their polarisation point on the polarisation sphere. The source position and the corresponding geometric locus of the polarisation point are printed in same brightness.

is verified. Adopting the decomposition

$$\hat{\mathbf{p}}^{(i)} = A \mathbf{e}_r^{(i)} + B \hat{\mathbf{s}} + C \hat{\mathbf{t}}^{(i)} \quad (3)$$

where $\hat{\mathbf{t}}^{(i)} = (\mathbf{e}_r^{(i)} \times \hat{\mathbf{s}}) / |\mathbf{e}_r^{(i)} \times \hat{\mathbf{s}}|$, a straightforward calculation involving the normalisation of vectors, the transversity of polarisation vectors and the condition for being inside the spherical cap leads to the arc length $L^{(i)}$ of the geometric locus lying inside the considered area. The result takes a simple form in terms of $\tau^{(i)} \in [0, \pi[$, the angle between $\mathbf{e}_r^{(i)}$ and $\hat{\mathbf{s}}$: condition (2) becomes $\sin \tau^{(i)} \geq \cos \eta$ and, by integration, the arc length is found to be:

$$L^{(i)} = \begin{cases} 2 \arccos \left(\frac{\cos \eta}{\sin \tau^{(i)}} \right) & \text{if } \sin \tau^{(i)} \geq \cos \eta \\ 0 & \text{otherwise} \end{cases} \quad (4)$$

Therefore, the probability $\ell^{(i)}$ that the i -th source of the sample leads to a polarisation point inside a spherical cap is given by:

$$\ell^{(i)} = \frac{L^{(i)}}{\pi}. \quad (5)$$

As it is explicitly shown, these probabilities only depend on the chosen aperture angle of the spherical cap and on the angle between the source positions and the cap centre. These probabilities are thus completely independent of the system of coordinates.

For each cap, the set of probabilities $\ell^{(i)}$ leads to the construction of the probability distribution P_n of

observing exactly n points of polarisation inside the spherical cap. If N is the sample size we have:

$$P_0 = \prod_{i=1}^N (1 - \ell^{(i)}) \quad (6)$$

$$P_1 = \sum_{j=1}^N \ell^{(j)} \prod_{i \neq j} (1 - \ell^{(i)}) \quad (7)$$

$$P_2 = \frac{1}{2} \sum_{k=1}^N \ell^{(k)} \sum_{j \neq k} \ell^{(j)} \prod_{i \neq j \neq k} (1 - \ell^{(i)}) \quad (8)$$

\vdots

$$\begin{aligned} P_N &= \frac{1}{N!} \sum_{l=1}^N \ell^{(l)} \dots \sum_{j \neq \text{prev. indices}} \ell^{(j)} \prod_{i \in \{\emptyset\}} (1 - \ell^{(i)}) \\ &= \prod_{l=1}^N \ell^{(l)} \quad . \end{aligned} \quad (9)$$

Note that following the previous definitions, it is possible to write, for each n ,

$$P_n = \frac{1}{n} \sum_{j=1}^N \ell^{(j)} P_{n-1 \setminus j} \quad (10)$$

where $P_{n-1 \setminus j}$ is the probability to observe $n-1$ points of polarisation (and only $n-1$) after the j -th element is removed from the original sample, making the new sample size $N-1$.

2.2 A fast algorithm for generating the P_n

Starting with the entire sample of size N , let consider the probability P_0 to observe no polarisation point within the cap. We remove the k -th element from this sample. Then, from equation (6), the probability to observe no polarisation point within this reduced sample, denoted by $P_{0 \setminus k}$, is related to P_0 through $P_0 = \ell^{(k)} P_{0 \setminus k}$, where we introduced the following notation for the probability that the source k does not lead to a polarisation point in the concerned area : $\ell^{(k)} \equiv (1 - \ell^{(k)})$.

First consider the probability P_1 to observe one and only one polarisation point:

$$\begin{aligned} P_1 &= \sum_{j=1}^N \ell^{(j)} \prod_{i \neq j} \ell^{(i)} \\ &= \sum_{j=1}^N \ell^{(j)} P_{0 \setminus j} \\ &= \sum_{j \neq k} \frac{\ell^{(j)}}{\ell^{(j)}} P_0 + \ell^{(k)} P_{0 \setminus k} \\ &= \ell^{(k)} \left(\sum_{j \neq k} \frac{\ell^{(j)}}{\ell^{(j)}} P_{0 \setminus k} \right) + \ell^{(k)} P_{0 \setminus k} \\ &= \ell^{(k)} P_{1 \setminus k} + \ell^{(k)} P_{0 \setminus k} \quad . \end{aligned} \quad (11)$$

A similar calculation leads to $P_2 = \ell^{(k)} P_{2 \setminus k} + \ell^{(k)} P_{1 \setminus k}$. One can prove by induction that the following relation holds:

$$P_m = \ell^{(k)} P_{m \setminus k} + \ell^{(k)} P_{m-1 \setminus k} \quad (12)$$

Table 1: The three regions of alignment of in equatorial coordinates B1950.

region	declination	right ascension	redshift	number of quasars
A1	$\delta \leq 50^\circ$	$168^\circ \leq \alpha \leq 217^\circ$,	$1.0 \leq z \leq 2.3$	56
A2	$\delta \leq 50^\circ$	$150^\circ \leq \alpha \leq 250^\circ$	$0.0 \leq z < 0.5$	53
A3		$320^\circ \leq \alpha \leq 360^\circ$	$0.7 \leq z \leq 1.5$	29

Assuming the relation is true for $m \leq n - 1$, it is easy to show that it is then true for $m = n$:

$$\begin{aligned}
P_n &= \frac{1}{n} \sum_{l=1}^N \ell^{(l)} P_{n-1 \setminus l} \\
&= \frac{1}{n} \sum_{l \neq k} \ell^{(l)} P_{n-1 \setminus l} + \frac{1}{n} \ell^{(k)} P_{n-1 \setminus k} \\
&= \cancel{\ell^{(k)}} \left(\frac{1}{n} \sum_{l \neq k} \ell^{(l)} P_{n-1 \setminus l \setminus k} \right) \\
&\quad + \ell^{(k)} \left(\frac{1}{n} \sum_{l \neq k} \ell^{(l)} P_{n-2 \setminus l \setminus k} \right) + \frac{1}{n} \ell^{(k)} P_{n-1 \setminus k} \\
&= \cancel{\ell^{(k)}} P_{n \setminus k} \\
&\quad + \ell^{(k)} \left(\frac{n-1}{n} \left[\frac{1}{n-1} \sum_{l \neq k} \ell^{(l)} P_{n-2 \setminus l \setminus k} \right] \right) \\
&\quad + \ell^{(k)} \frac{1}{n} P_{n-1 \setminus k} \\
&= \cancel{\ell^{(k)}} P_{n \setminus k} + \ell^{(k)} P_{n-1 \setminus k} \quad .
\end{aligned} \tag{13}$$

Therefore, equation (12) holds¹ for every $m \in \mathbb{N}$. Assuming that, for a sample of size N and for a given spherical cap, we possess all elementary probabilities $\ell^{(i)}$, we use the following algorithm² for numerically computing the probability density distribution:

- 1) We introduce a column vector V of size $N + 1$, initialized to zero, except for V_0 which is set to 1. The V_n are the P_n for an empty data set.
- 2) We add one data point at a time, and update V according to equation (12).
- 3) After N iterations, the V_n give the P_n distribution for the studied sample.

2.3 A first example

To illustrate the use of the above, we show in Fig. 2 a map of the expected background for region A1 of [Hutsemékers et al. 2005], as defined in Table 1.

At each point a of the polarisation sphere we associate a probability density distribution P_n^a through the use of spherical caps. The mean values $\bar{N}^a = \sum_n n P_n^a$ determine the most expected number of polarisation points. From those numbers, we build iso-density regions on the polarisation sphere in order to visualize the structure that the statistical background takes. We arbitrarily choose here caps of half aperture $\eta = 17^\circ$. The dependence of the results on η will be discussed in section 2.4.3.

Due to the non uniformity of the source locations, there are regions of maxima (and minima) in the expected densities of polarisation points as well as regions where polarisation points are forbidden. For this sample, a close look at Fig. 2 shows that a quadrupole is naturally expected in the density structure on the polarisation sphere. This shows that the use of the P_n distributions is mandatory, as the expected density is not flat.

¹Equation (12) was first introduced by Howard (1972) and its numerical behaviour was extensively discussed in the paper [Chen & Liu, 1997] about computational techniques for the Poisson-binomial probabilities. The algorithm presented here is equivalent to that given in [Chen & Liu, 1997].

²We have tested our implementation of the algorithm by comparing its results to those obtained via a Monte-Carlo treatment, for the A1 region of reference [Hutsemékers et al. 2005]. We produced 10000 random samples, for which the quasar positions were kept fixed and for which the polarisation angles were randomly generated according to a uniform distribution. For different spherical caps we built the corresponding P_n distributions, and found a perfect agreement. We checked that the same conclusions are obtained for the whole sample of quasars presented in [Hutsemékers et al. 2005] and for arbitrary sub-samples.

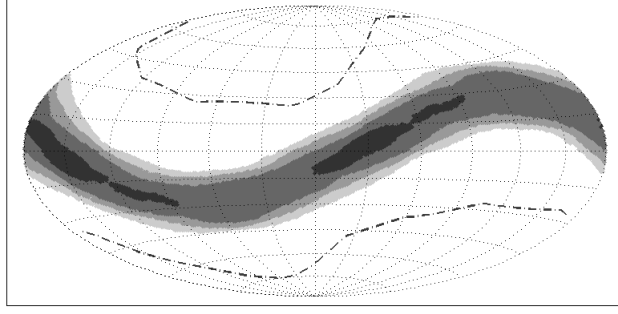


Figure 2: Hammer-Aitoff projection (galactic coordinates) of the polarisation sphere associated to the A1 region. Expected density regions are displayed following the legend: white: $\bar{N}^a < 4$; light grey: $4 \leq \bar{N}^a < 5$; grey: $5 \leq \bar{N}^a < 6$; dark grey: $6 \leq \bar{N}^a < 7$; black: $\bar{N}^a \geq 7$. White regions towards poles which are delimited by dashed curves are regions where polarisation points cannot fall at all.

2.4 Further refinements of the method

2.4.1 Optimal set of centres for the spherical caps

The method presented so far has two problems:

- Several spherical caps can contain the same polarisation points, so that several probability distributions are assigned to the same set of data points.
- Among the caps containing the same data points, the most significant ones will be those for which several of the $\ell^{(i)}$ will be small, i.e. for which the loci of several polarisation points are almost tangential to the caps. This enhanced significance is an artefact of our method.

In order to minimize these problems, we do not allow all caps to be considered, but rather focus on those that correspond to cones with an axis along the vectorial sum of the normalised polarisation vectors inside them. Hence the polarisation vector corresponding to the centre of the cap is

$$\mathbf{s}_{centre} = \sum_{i \in cap} \hat{\mathbf{p}}^{(i)}, \hat{\mathbf{s}}_{centre} = \frac{\mathbf{s}_{centre}}{|\mathbf{s}_{centre}|}$$

These centres are first determined by iteration before applying the algorithms explained above.

2.4.2 Local p-value of the data

The study of alignments is performed separately for each cap a on the polarisation sphere, for which we derive probability distributions P_n^a . In each cap, we count the number o_a of observed polarisation points, and $P_{o_a}^a$ gives us the probability that the presence of o_a polarisation points in cap a is due to a background fluctuation. The probability that a generation from a uniform background has a density greater than the observed one is given by the p-value $p^a = \sum_{n \geq o_a} P_n^a$. The latter quantity gives us the significance level of a specific polarisation point concentration in one given direction. As already mentioned, equation 5 shows that p is coordinate invariant. It in fact provides a generalisation of the binomial test used in [Hutsemékers 1998, Hutsemékers & Lamy, 2001, Hutsemékers et al. 2005]. For each sample, we can consider the cap a_{min} that gives the most significant p-value $p_{min} = \min_a(p^a)$ which we shall call the significance level. This defines a direction in the polarisation space, and a plane in position space.

2.4.3 Dependence on the spherical cap aperture

The only free parameter in this method is the aperture half-angle of the spherical caps. Results will depend on its value and one should choose it to optimize the detection of the signal, i.e. to decrease p_{min} .

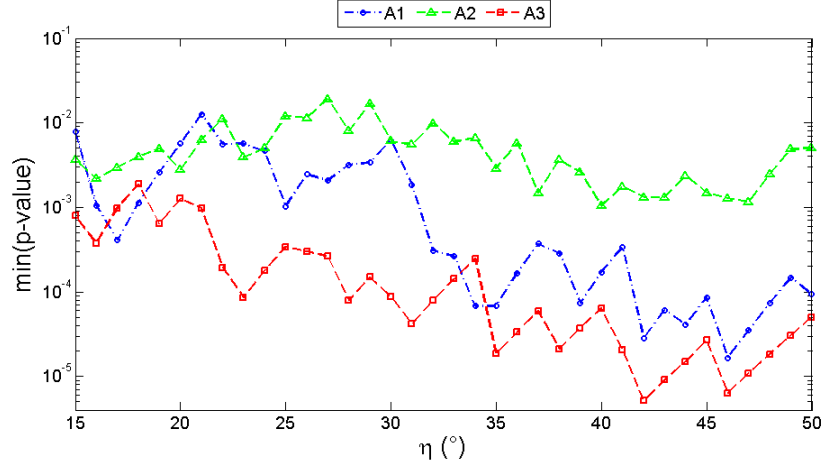


Figure 3: Dependence of the significance level with η , the half-aperture angle of spherical caps (in degree). The regions are defined as in Table 1

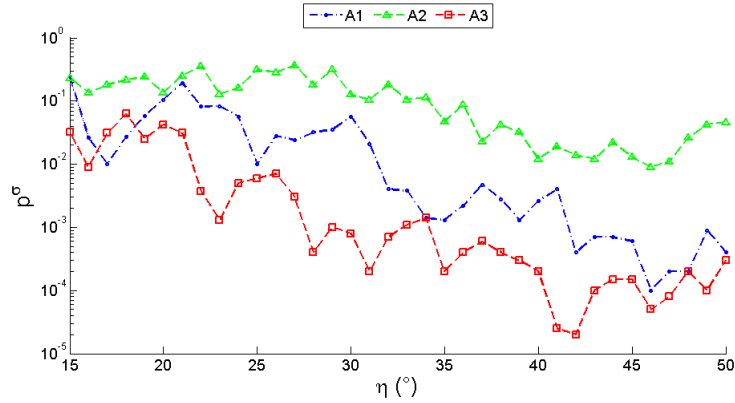


Figure 4: Behaviour of the global significance level with the half-aperture angle for the A1, A2 and A3 regions of Table 1

For a given sample of sources we perform the study for a wide range of half-aperture angle. For each of them we determine the optimum cap centres, and calculate p_{min} as a function of η . Fig. 3 shows p_{min} as a function of η for sub-samples A1, A2 and A3, as defined in [Hutsemékers et al. 2005], for η taking all integer values between 15 and 50 degree.

Fig. 3 shows that the different samples present significant over-densities of polarisation points. We see that p_{min} is smaller for η between 30° and 50°, depending on the sample. We shall now see that another criterion must be taken into account before we fix η .

2.4.4 Global significance level of the effect

So far, we have considered the probability that an over-density in a given cap be due to a background fluctuation. A more relevant probability maybe that of the occurrence of such an over-density anywhere on the polarisation sphere. To calculate this, we have resorted to a Monte-Carlo treatment, generating for each data sample N_s simulated datasets, in which we consider only the quasars of that dataset, fix their positions on the sky, and randomly vary their polarisation angles according to a flat distribution. For a given data sample, we introduce a global significance level p^σ defined as the proportion of random sets which produce p -values smaller or equal to p_{min} somewhere on the polarisation sphere.

Table 2: Significance levels for various data samples.

region	P_{bin}	p_{min}	$\eta(^{\circ})$	o_a/o_a^{max}	p^{σ}
A1	$3.3 \cdot 10^{-6}$	$1.7 \cdot 10^{-5}$	46	43/56	$1.0 \cdot 10^{-4}$
A2	—	$1.7 \cdot 10^{-3}$	46	32/47	$0.9 \cdot 10^{-2}$
A3	$2.6 \cdot 10^{-5}$	$5.1 \cdot 10^{-6}$	42	25/29	$2.7 \cdot 10^{-5}$

o_a is the number of polarisation points inside the spherical cap where the minimum significance level (minimum p-value) p_{min} is observed, o_a^{max} is the maximum number of polarisation points that might fall inside this cap. η is the half-aperture angle of the cap. P_{bin} is the binomial probability obtained in [Hutsemékers et al. 2005] (Table 1) and p^{σ} is the global significance level of the region obtained through the method explained in section 2.4.4.

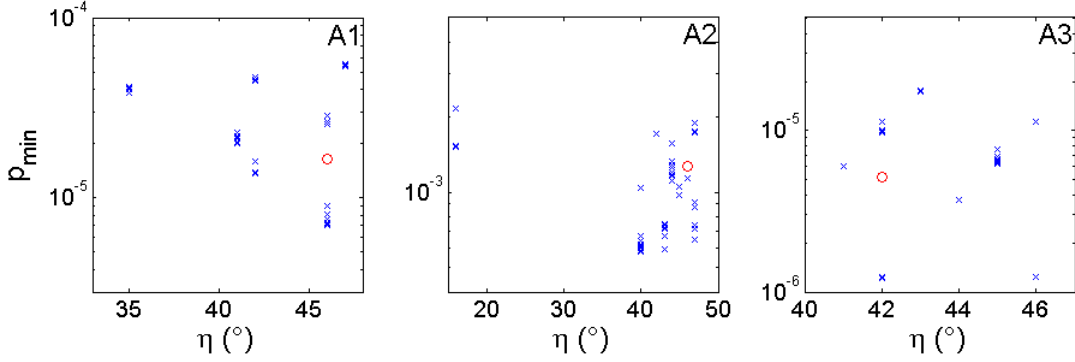


Figure 5: Result of the Jackknife methods for regions A1, A2 and A3. The red circles correspond to the results of Table 2.

2.4.5 Optimal angle for the spherical caps

Fig. 4 shows the behaviour of the global significance level p^{σ} with the aperture angle of the spherical caps for the sub-samples A1, A2 and A3. Comparing Figs. 3 and 4, we note that p^{σ} and p_{min} follow the same trend. Clearly, the relation between them must involve the number of possible caps N_c , and p^{σ} would be equal to $N_c p_{min}$ if the caps did not overlap and if all simulated datasets had the same number of caps. Hence we expect N_c to be of the order of the area of the half-sphere divided by the area of a cap, $p^{\sigma} \approx p_{min} / (1 - \cos\eta)$. We found empirically that this relation underestimates p^{σ} by a factor smaller than 4, for all the samples we analysed.

Table 2 shows the significance levels p_{min} of over-densities obtained for the different samples of quasars, compared with those reported in [Hutsemékers et al. 2005]. Note that a spherical cap is in general sensitive only to sources along a band of the celestial sphere so that only part of the entire data sample can contribute to it. We thus compare the number of polarisation points in the cap o_a to the maximum number of points possible in that cap, o_a^{max} .

We see from Table 2 that the best half-aperture angle depends on the region, and that it is large: 42 or 46 degrees.

We also see that the regions A1 and A3 defined in [Hutsemékers et al. 2005] are the most significant with our algorithm. However, we need to know whether the difference between P_{bin} and p_{min} is important. We shall then study the errors on the significance level and on η and see that the discrepancies are reasonable.

To do so, we perform a Jackknife analysis, removing in turn each quasar from a given sample, and performing the analysis again. The results are shown in Fig. 5.

We see that the errors on η are large, and that p_{min} can go up or down by a factor of the order of 3. Hence it seems that our method really agrees with the estimates of [Hutsemékers et al. 2005]. One also clearly sees that region A2 is less significant than A1 and A3. In the following, given the large uncertainties, we choose to fix the angle η at 45° . Note that the local and global significance levels we give could be slightly improved if we chose a different value of η for each sample.

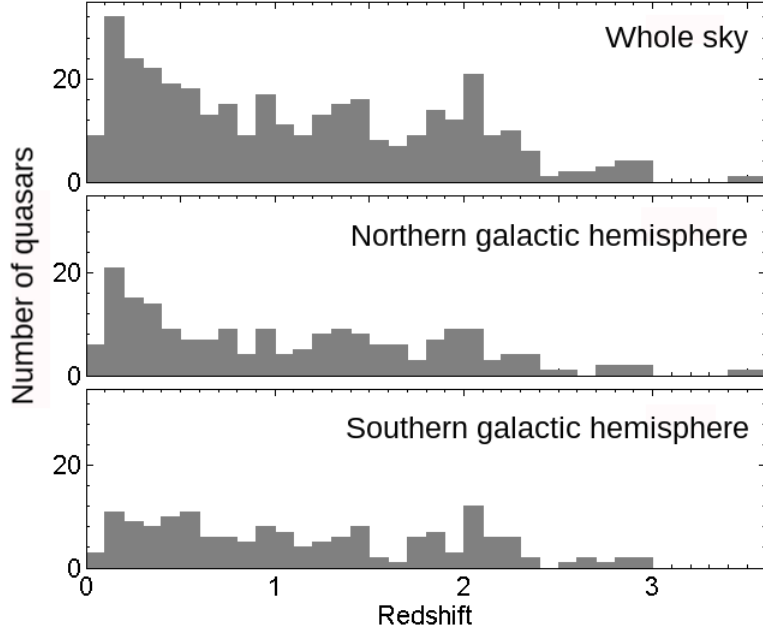


Figure 6: The redshift distribution of the sample of 355 quasars with bin width of $\Delta z = 0.1$ are shown for the whole sky, the northern galactic hemisphere and the southern galactic hemisphere. The last bin in the whole sky and northern histograms contains the quasar at $z = 3.94$.

Table 3: Parameters of the most significant caps.

Sample	p_{min}	$(\delta, \alpha)_{a_{min}} (^\circ)$	o_a/o_a^{max}	$(\delta, \alpha)_{\langle \mathbf{e}_r \rangle} (^\circ)$
Whole	$1.5 \cdot 10^{-2}$	(48.6, 283.7)	163/318	(5.5, 185.0)
Northern sky	$9.3 \cdot 10^{-2}$	(23.1, 294.0)	82/173	(12.2, 197.2)
Southern sky	$5.1 \cdot 10^{-5}$	(39.7, 270.6)	89/142	(-0.7, 358.5)

3 Results

We now have a coordinate-invariant statistical test which depends only on the half-aperture angle of the caps and which takes into account the dispersion of sources on the sky. We can now scan the full sample, or sub-samples with various cuts, to check whether we detect significant alignments.

3.1 Full sample

Here we consider the full sample of quasars. Because the observations are away from the galactic plane, they are split into North and South, so that we shall also consider all the northern quasars or all the southern ones. Each sample has respectively 355, 195 and 160 sources. We show their redshift distribution in Fig. 6. We consider all the possible spherical caps, and show the most significant ones in Table 3. The first column gives the most significant p-value, the equatorial coordinates in the polarisation space $(\delta, \alpha)_{a_{min}}$ of the centre of the most significant cap, and the ratio o_a/o_a^{max} . We also give the angular coordinates of the vector $\langle \mathbf{e}_r \rangle$ resulting from the normalized sum of the position vectors of the o_a sources in the last column. This is the first result of this paper. We see here that a global southern alignment seems to be detected. This being said, the alignment could be caused by a subregion in redshift, and hence we shall now consider this question.

3.2 Redshift dependence

It has been reported in [Hutsemékers & Lamy, 2001, Hutsemékers et al. 2005, Hutsemékers et al. 2008, Hutsemékers et al. 2009, Jain, Narain & Sarala, 2004] that the direction of large-scale alignments of optical polarisation orientations of quasars shows a dependence on the redshift of the sources. In order to study this question, we consider

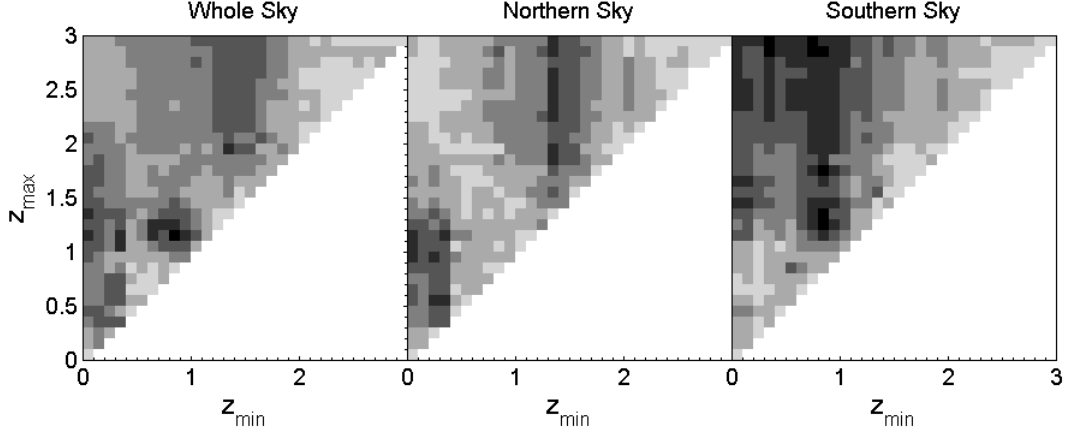


Figure 7: Contour plots of p_{min} as a function of the minimum and maximum values of the redshift, for the whole sample, for the galactic North and for the galactic South. Values from 10^{-6} to 10^{-5} are in black, and the different nuances of grey correspond to factors of 10, up to the white regions, which are for p_{min} between 0.1 and 1.

the data between two redshifts z_{min} and z_{max} and vary the latter by steps of 0.1 (we also exclude the one quasar with $z > 3$). As our test does not use the quasar position (although it depends on it), we do not need to introduce further cuts by hand as in [Hutsemékers 1998, Hutsemékers et al. 2005]. We nevertheless consider the whole sample, or the northern and southern regions separately. We show in Fig. 7 the result of this study. Clearly, the dependence on redshift does not seem to be continuous: the alignment is present for some redshifts and not for others. In particular, all regions present alignments at small z_{min} , the northern hemisphere has one further clear alignment starting at $z = 1.3$, whereas the southern hemisphere has a significant alignment starting at $z = 0.8$. The alignments detected in the whole sample originate from alignments present in the northern or southern samples, and no new region seems to be present. We give the parameters of the most significant caps for each region in Table 4, where W, N and S stand for whole sky, North and South. Region W0 is seen to be created by the northern alignment N0, and region W1 comes from the southern alignment S2. We shall discuss region WCo later in section 3.3. To the South, S0, S1 and S2 point in the same direction in polarisation (remember that the caps have a half aperture of 45°), and are in same direction in the sky. So it seems that there is an effect concentrated in the region $0.8 < z < 1.3$ (note that almost all the available quasars are aligned), but extending to redshifts as high as 3 and as low as 0.3. To the North, the alignment effect is less significant, and there are two directions of polarisation, different from that of S1 or S2. Similarly, regions N0 and N1 are close in direction in polarisation and position, whereas N2 is independent. Furthermore, the directions of strongest alignment (in the polarisation space) change strongly from low (N0 or N1) to high redshift (N2): the angular change is of the order of 70° , which is reminiscent of results already obtained in [Hutsemékers et al. 2005]. Note that the region N2 overlaps with the A1+ region defined in [Hutsemékers et al. 2005]. We shall discuss these points further in the next subsection.

3.2.1 Fine structure

We can explore the structure of each region by slicing it into sub-samples, according to linear polarisation, redshift, right ascension or declination. We show the result of this study in Fig. 8, for the samples defined in Table 4. One can see that there is no evidence that the alignment is more manifest for sources with a small degree of linear polarisation. Cutting off the large values of p_{lin} negligibly reduces p_{min} for regions N1 and S2. The redshift structure is flat, except for region S0 or S1, for which the contributions of various redshifts seem randomly arranged, hence it seems that region S2 is likely the true region of southern alignment.

3.2.2 Best regions

The dependence on right ascension and declination suggests that some regions of the sky are more significantly aligned. From this observation, we can define even more significant regions, by placing cuts on right ascension and declination. This does not lead to a significant difference, except for regions N2 and S2. Following the above argument, it seems we have detected three independent regions of alignment, which are significant. We summarise their parameters in Table 5. Note that N0, N2+ and S2+ are improved versions of A2, A1+ and

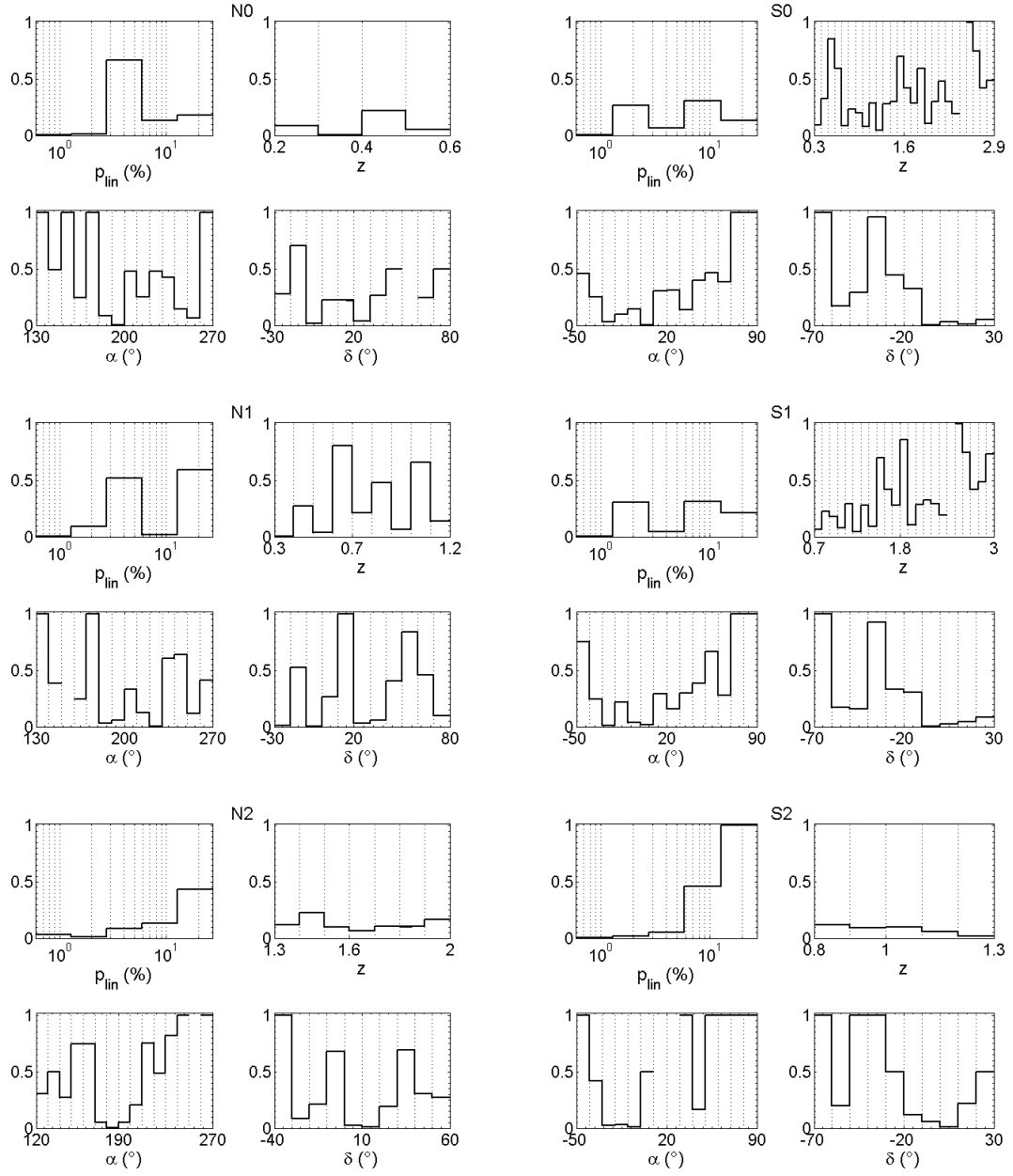


Figure 8: Fine structure of samples N0, N1, N2, S0, S1 and S2.

Table 4: Significant sub-samples from the scan on redshift performed on the whole sample of 354 quasars and the northern and southern samples of 194 and 160 sources, respectively.

Sample	z_{min}	z_{max}	p_{min}	p^σ	$(\delta, \alpha)_{a_{min}} (^\circ)$	o_a/o_a^{max}	$(\delta, \alpha)_{(e_r)} (^\circ)$
W0	0.3	1.1	$2.9 \cdot 10^{-5}$		(20.7, 304.3)	60/99	(16.9, 203.3)
W1	0.8	1.2	$7.3 \cdot 10^{-6}$		(25.4, 278.1)	31/40	(12.2, 181.2)
WCo	1.3	2.0	$4.3 \cdot 10^{-6}$	4/150000	(65.9, 293.1)	39/50	(-9.3, 3.5)
N0	0.2	0.6	$1.4 \cdot 10^{-5}$	9/50000	(15.0, 308.2)	28/37	(22.3, 208.4)
N1	0.3	1.2	$1.5 \cdot 10^{-5}$		(12.7, 305.0)	40/58	(19.3, 206.4)
N2	1.3	2.0	$3.5 \cdot 10^{-5}$	17/50000	(78.2, 298.1)	35/47	(5.8, 186.6)
S0	0.3	2.9	$8.1 \cdot 10^{-6}$		(44.7, 273.8)	79/120	(-5.0, 357.1)
S1	0.7	3.0	$3.1 \cdot 10^{-6}$		(43.6, 272.3)	62/89	(-7.0, 357.6)
S2	0.8	1.3	$3.9 \cdot 10^{-6}$	3/100000	(31.8, 263.9)	19/20	(-7.8, 348.3)

Best cap parameters are shown as in Table 3 as well as the lower and upper limits in redshift of sub-samples. Note that region WCo is detected for $p_{lin} \leq 1.5\%$. Boxes stress the most significant independent regions (see text for a discussion). The p^σ values are given in format n_c/N_s where n_c is the number of Monte-Carlo simulations that show a significance level lower than that of the data, among the N_s we have performed.

Table 5: Best independent regions of alignment.

Sample	z_{min}	z_{max}	p_{min}	$(\delta, \alpha)_{a_{min}} (^\circ)$	o_a/o_a^{max}	δ interval ($^\circ$)	α interval ($^\circ$)
N0	0.2	0.6	$1.4 \cdot 10^{-5}$	(15.0, 308.2)	28/37	$[-25, 80]^*$	$[135, 265]^*$
N2+	1.3	2.0	$4.5 \cdot 10^{-6}$	(79.8, 289.3)	30/35	$[-30, 35]$	$[165, 230]$
S2+	0.8	1.3	$1.9 \cdot 10^{-6}$	(31.80, 261.2)	18/18	$[-55, 25]^*$	$[-40, 40]$

The regions in δ, α marked by an asterisk describe the data sample, the others are cuts imposed on the data.

A3 defined in [Hutsemékers et al. 2005].

3.3 A possible cosmological alignment

Although cutting on polarisation does not improve significantly the previous probabilities, we detected a rather surprising alignment, as it is very significant only when the North sample is considered together with the southern one. Indeed, if we consider only small linear polarisations, with $p_{lin} \leq 1.5\%$, then there is a North-South alignment with a $p_{min} < 5 \cdot 10^{-6}$, as shown in the sample WCo of Table 4. This alignment is much less significant in the North ($p_{min} \approx 2 \cdot 10^{-4}$) or in the South ($p_{min} \approx 10^{-3}$), but it becomes significant once both hemispheres are considered together. It must also be noted that it is significant only after the cut on linear polarisation.

3.4 A naive interpretation

One can imagine that a systematic oscillating electric field \mathbf{E} is at work in each of the regions we defined. We can try to determine its norm and take it parallel to the centre of the polarisation cap $\hat{\mathbf{s}}_{centre}$, in such a way that the alignments we found disappears if we subtract that systematic effect from the samples we defined (in practice we impose that $p_{min} \geq 0.1$). Of course, we have first to project \mathbf{E} onto the plane normal to the direction of propagation, then add it to the polarisation. If we perform this exercise, the resulting values of $|\mathbf{E}|$ are given in Table 6 for the most significant regions of Table 4. It is remarkable that the vectors we have to remove from the data have roughly the same norm. Due to the projection of the vector \mathbf{E} , this naive model could explain why polarisation vectors are not all seen to be aligned.

Table 6: Norm of a systematic 3-vector accounting for the effect.

Sample	$ E $ (%)
N0	0.65 – 0.70
N2	0.6 – 0.7
S2	0.8 – 1.2
WCo	0.5 – 0.9

4 Conclusion

We have presented in this paper a new coordinate-invariant method to detect polarisation alignments in sparse data, and applied it to the case of alignments of optical polarisation vectors from quasars. We showed that we automatically recover regions previously found, and we refined their limits based on objective criteria (see Table 5). As a byproduct, the directions of alignments in space are unambiguously determined. The method we propose is powerful, as the coordinate-invariant significance levels are semi-analytically determined. The remaining drawback is that the determination of the global significance levels relies on very time-consuming Monte-Carlo simulations. We believe that this new analysis puts the alignment effect on stronger grounds, as it is now significant at the $3 \cdot 10^{-5}$ level. However, one has to note that the significance levels obtained in this papers and those reported in [Hutsemékers et al. 2005] are not in full agreement. Indeed, the Z-type tests used in [Hutsemékers 1998] and [Jain, Narain & Sarala, 2004] reshuffle the measured polarisation directions while keeping the source locations to evaluate the background. The advantage is that any systematic effect vanishes automatically through this method. The disadvantage is that it washes out global effects, or alignments present for a large number of quasars. Our method has the opposite features: we can detect global alignments, but we are sensitive to systematic effects. Hence the two methods do not need to be in full agreement. Applying our method to the sample of 355 quasars compiled in [Hutsemékers et al. 2005], we identified the following main features. The directions of alignments show a dependence on the redshift of the sources. Although this dependence seems discontinuous, one should note that we detected significant alignments for redshift intervals where the distribution of data peaks. Thus, more data in regions of redshift with poor statistics are required in order to study this dependence in more details. As seen in Fig. 8, for a given redshift interval, alignment seems to be mainly due to quasars well localized toward specific directions of the sky. Furthermore, no strong evidence has been found for a dependence on the degree of linear polarisation. As a result and in agreement with [Hutsemékers et al. 2005], based on the present sample, we established two distinct regions towards the North galactic pole, one at low and the other at high redshift, and only one towards the South galactic pole at intermediate redshift, which possibly dominates the whole southern sky. Besides the regions previously detected, or their improved version, we also showed that there exists the possibility of a cosmological alignment.

5 Acknowledgements

We would like to thank D. Hutsemékers for many helpful comments, suggestions and discussions.

References

- [Chen & Liu, 1997] Chen, S. X., Liu J. S., 1997, *Statistica Sinica*, 7, 875-892.
- [Eisenberg & Guy, 1979] Eisenberg, M., Guy, R., 1979, *The American Math. Mon.* 86 (7): 571–574.
- [Howard 1972] Howard, S., 1972, *J. Roy. Statist. Soc. Ser. B* 34, 2012-211.
- [Hutsemékers 1998] Hutsemékers, D., 1998, *A&A*, 332, 410.
- [Hutsemékers & Lamy, 2001] Hutsemékers, D., Lamy, H., 2001, *A&A*, 367, 381.
- [Hutsemékers et al. 2005] Hutsemékers, D., Cabanac, R., Lamy, H., Sluse, D., 2005, *A&A*, 441, 915.
- [Hutsemékers et al. 2010] Hutsemékers, D., Borguet, B., Sluse, D., Cabanac, R., Lamy, R., 2010, *A&A*, 520, id L7.

- [Hutsemékers et al. 2008] Hutsemékers, D., Payez, A., Cabanac, R., Lamy, H., Sluse, D., Borguet, B., Cudell, J.-R., 2008, in Bastien, P., (Ed.) *Astronomical Polarimetry 2008: Science from Small to Large Telescopes*, ASPC 449 (2011, November 01)
- [Jain, Narain & Sarala, 2004] Jain, P., Narain, G., Sarala, S., 2004 MNRAS, 347, 394.
- [Sluse et al. 2005] Sluse, D., Hutsemékers, D., Lamy, H., Cabanac, R., Quitana, H., 2005, A&A, 433, 757